Chapter - 6

Zirconium tungstate and it's bionanocomposite with Chitosan - a catalyst for degradation of Single and Binary mixture of dyes

6.1 Introduction

Catalytic oxidation using hydrogen peroxide was found to be superior in comparison with other methods [1-5] for degradation of recalcitrant dyes [1, 6-8]. Amongst the various catalysts being used for degradation of dyes, ion exchange materials as catalysts are highly specific and selective for water treatment studies due to which scientists opt to exploit these materials for various applications [9, 10].

Zirconium Tungstate belongs to the cubic AM_2O_8 family (A=Zr, Hf; M=Mo, W). The tungstates are thermodynamically stable at high temperatures [11, 12]. Zirconium tungstate (ZrW_2O_8) is an unique ceramic oxide that exhibits a negative coefficient of thermal expansion (CTE) over a wide temperature range [13]. ZrW_2O_8 (ZrW) based materials have been used in a wide range of applications such as, low CTE polymer composites [14–17], substrates for mirrors and optical devices [18], microelectronics [19, 20] and construction materials [21]. ZrW_2O_8 was also discovered to be a novel photocatalyst for hydrogen production from photocatalytic water splitting [22].

The synthesis of ZrW_2O_8 nanoparticles has been attempted through either sol–gel [23, 24] or hydrothermal methods [25–27]. Sullivan and Lukehart [23] reported a sol–gel/reverse micelletechnique, which resulted in parallelepiped nanoparticles. Zhang et al. [24] also utilized the sol–gel technique for the synthesis of ZrW_2O_8, which were further electro spinned to produce ZrW_2O_8 nanofibers. Xing et al. [25] used a hydrothermal method in HCl medium for synthesis of ZrW_2O_8 nanorods with widths ranging from 40 to 500 nm. Kozy et al. [26] obtained smaller ZrW_2O_8 nanoparticles of different morphologiesthrough careful control of hydrothermal reaction variables such as nature of acid, concentration and reaction time. C.A. Perottoni et al [28, 29] have shown that ZrW_2O_8 undergoes an irreversible pressure-induced amorphization above 1.5 GPa. The amorphous phase ofzirconium tungstate reverts to α-ZrW_2O_8 upon annealingat about 900 K at ambient pressure [28].

Of all the methods the sol –gel/hydrothermal method seems to be the best due to its ease in processing methodology and control on the morphology of the particles [30-33]. Furthermore, ZrW can be incorporated into various biopolymer matrix materials to produce composites to be utilized in a wide range of applications [34-38]. The incorporation of the catalyst onto the surface of a polymer provides the best performance with an extensive potential for reuse. Hongchao et.al had utilized Zirconium Tungstate/Epoxy Nanocomposites [39] for the application in microelectronic insulation industry. Niwas et.al had investigated the adsorption of phosphamidon on the surface of styrene supported zirconium (IV) tungstophosphate [40]. Natrayasamy Viswanathan and S. Meenakshi had investigated the adsorption of fluoride onto chitosan supported zirconium (IV) tungstophosphate composite [41]. These composite ion exchangers have the desired properties of both organic and inorganic counter parts put into one moleculewith the required selectivity, specificity as well as wide range of applicability, making them amenable for their use in environmental remediation. In this aspect chitosan, as already seen in previous chapters can be considered to be the best support due to its biocompatibility and biodegradability. Furthermore, the separation of nanocatalyst can be done efficiently if it is supported onto a biopolymer surface.

Hence, in the present study, an attempt has been made to prepare nano ZrW particles and its potential for catalytic degradation of dyes has been explored. Having been successfulin the preparation of nanoZrP (chapter 5) the autoclave method was used for the preparation of ZrW. Furthermore, a bionanocomposite of ZrW has been prepared using biopolymer chitosan to enhance the catalytic efficiency, selectivity and ease of recovery of catalyst after degradation of individual and mixture of dyes. The degradation of anionic dyes Reactive blue-21 (RB-21), Reactive red-141 (RR-141) and a cationic dye Rhodamine-6G (Rh-6G) have been investigated. The binary mixture of these dyes Reactive blue-21 +Reactive red -141 (RB+RR), Reactive Red 141 + Rhodamine-6G (RR+RH) and Reactive blue-21 + Rhodamine-6G (RB+RH) have also been investigated.

Preliminary investigations revealed that ZrW and CZrW did not show significant adsorption potential. The adsorption experiments were not performed further.

6.2 Materials and methods

Sodium tungstate (Na_2WO_4, Merck; 99.9%), Zirconium oxy chloride ($ZrOCl_2.8H_2O$, Spectrachem), Commercially used dyes Reactive blue-21 (RB-21), Reactive red-141 (RR-141), Rhodamine-6G (Rh6G) and hydrogen peroxide (H_2O_2, Fisher Scientific; 30%solution), were used in this study without further purification.

6.2.1 Synthesis of Zirconium tungstate and Chitosan/ Zirconium tungstate nanocomposite

Synthesis of Zirconium tungstate (ZrW)

Zirconium tungstate (ZrW) was prepared by adding an aqueous solution of sodium tungstate to an aqueous solution of zirconium oxychloride in 2:1 molar proportion, under stirring condition at room temperature. White precipitates of Zirconium tungstate is formed which was stirred for 2 hours for complete precipitation which was further kept in autoclave for 3 hours. The precipitates were then centrifuged and washed with conductivity water till the washings were chloride free and dried at 40ºC to obtain ZrW nanoparticles.

Synthesis of Chitosan-Zirconium tungstate nanocomposite (CZrW)

1% Chitosan solution(100 ml) in acetic acid was added to 10 g of synthesised Zirconium tungstate nanoparticle solution in stirring condition. After few minutes (~ 10 min) fibrous white coloured material was formed which was autoclavedfor 3 hrs to obtain chitosan /Zirconium tungstate nanocomposite (CZrW). The precipitates were then centrifuged and washed with conductivity waterand dried at 40ºC.

6.2.2 Individual and Binary dye degradation experiments

The respective individual solutions Reactive blue -21 (RB-21), Reactive red-141 (RR-141) and Rhodamine-6G (Rh-6G) and binary mixture of dye solutions (RB+RR, RR+RH, RB+RH) prepared by dissolving the required amount of dye in 100 mL of DDW. Samples were prepared by mixing 3 mL of the dye solution, 0.5 mg catalyst and 100 µL of 30% H_2O_2 in a cuvette. The cuvette was then inserted in the spectrophotometer, Scans were started immediately after the addition of nanoparticles, and the solution was left untouched until completion. Absorbance was monitored at the respective maximum wavelength.

6.2.3 Characterisation of the Zirconium tungstate and Chitosan – Zirconium tungstate materials

The synthesised ZrW and CZrW were characterised by FTIR, XRD, Raman Spectroscopic techniques as well as by TGA, TEM and EDS analysis. The details of the instruments and techniques are the same as mentioned in Chapter 2, section 2.13 and chapter 3 section 3.2.3.

6.3 Results and Discussion

6.3.1 FTIR spectroscopy

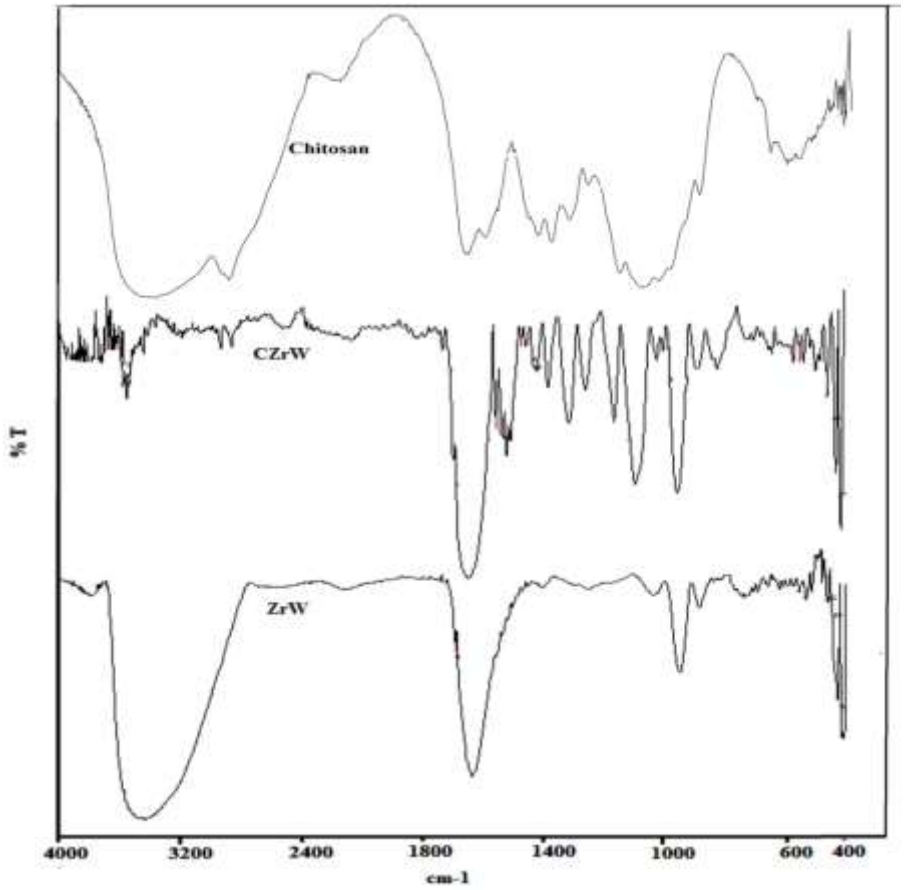

Figure 6.1 IR spectra of Chitosan, CZrW and ZrW and Chitosan

Figure 6.1 shows the FTIR spectra of Chitosan, CZrW and ZrW. The broad but strong peak in the region 3,600-3,000 cm^{-1}can be attributed to the O–H stretching of lattice water molecules in ZrW [42, 43] and free OH group stretching in chitosan.It can be seen that there is no such broad band in CZrW which could be due to the H-bonding between both chitosan and ZrW to form composite CZrW. The intense sharp peak at 1,634 and 1641 cm^{-1}in ZrW and CZrW may be due to H–O–H bending. The bending vibration peaks of -W-Oat 511 and 588 cm^{-1} has been shifted to 494 and 563

cm^{-1}in CZrW which indicates the interaction of ZrW with chitosan moiety. The bands in the regions 830-780 and 900-825 cm^{-1} can be assigned to $(WO_4)^{2-}$and metal oxide groups, respectively [44]. The bandsin the range 600- 400 cm^{-1} can be attributed to WO_4 asymmetric bending modes and stretching modes of ZrO_6 in ZrW and CZrW.

6.3.2 UV spectroscopy

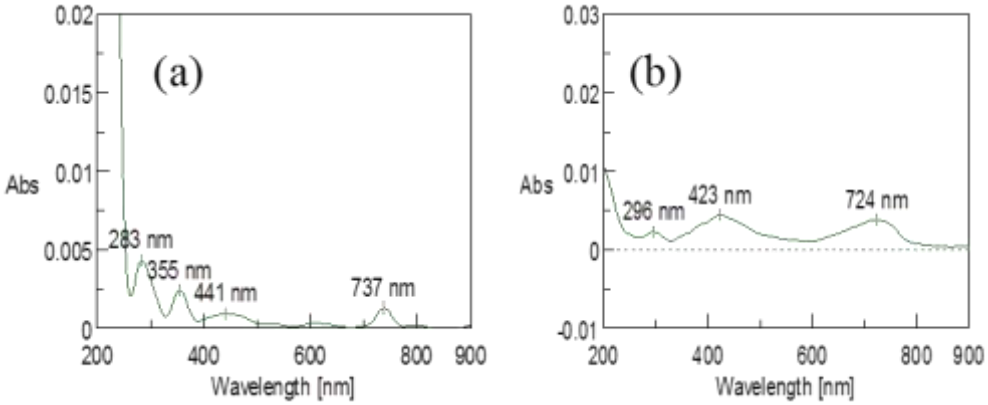

Figure 6.2 Solid UV Spectra of a) ZrW b) CZrW

Figure 6.2 (a & b) shows the UV spectra of ZrWand CZrW. The band gap energy of ZrW (4.39 eV) is large indicating that it could only utilize UV light irradiation. The absorption edge in the UV region is due to the excitation from O_{2p} to Wt_{2g} in WO_4^2. The large band gap could be attributedto small size and the quantumconfinement limiting which is expected forsemiconducting nanoparticles and the absorption edge will be shifted to highenergy with decrease in particle size [45, 46]. The band gap was reduced to a small extent in C-ZrW (4.2eV)

6.3.3 Morphology analysis (TEM and EDX)

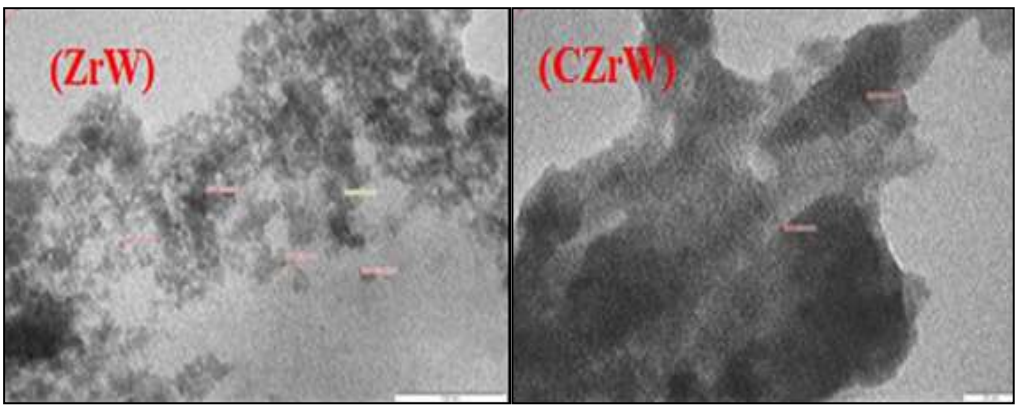

Figure 6.3 TEM images of ZrW and ZrW

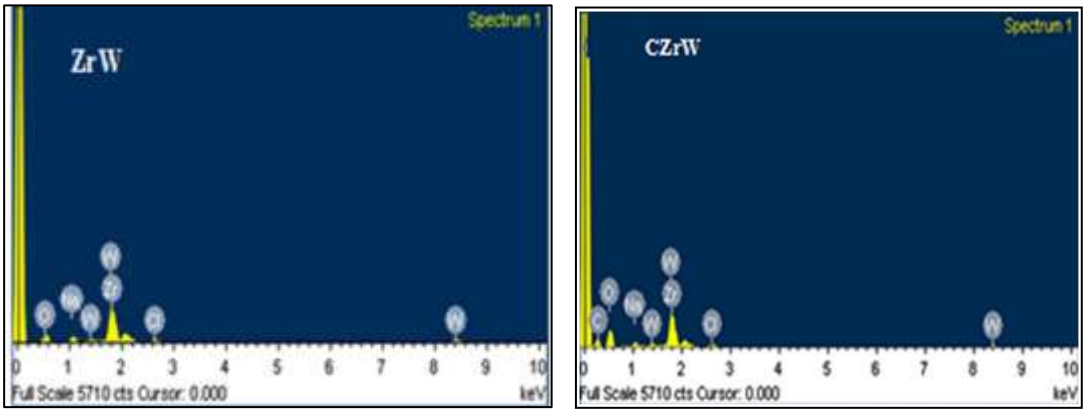

Figure 6.4 EDAX images of ZrW and CZrW

Figure 6.3 shows the TEM images of ZrW and CZrW composite. ZrW show cluster like irregular morphology with an average particle size was in the range (10 - 15 nm). The EDX spectrum shown in Figure6.4 confirmed that zirconium and tungsten were main components present in the both ZrW and CZrW along with carbon which is present only in CZrW further evidencing the formation of composite in case of CZrW.

6.3.4 X-Ray diffraction analysis

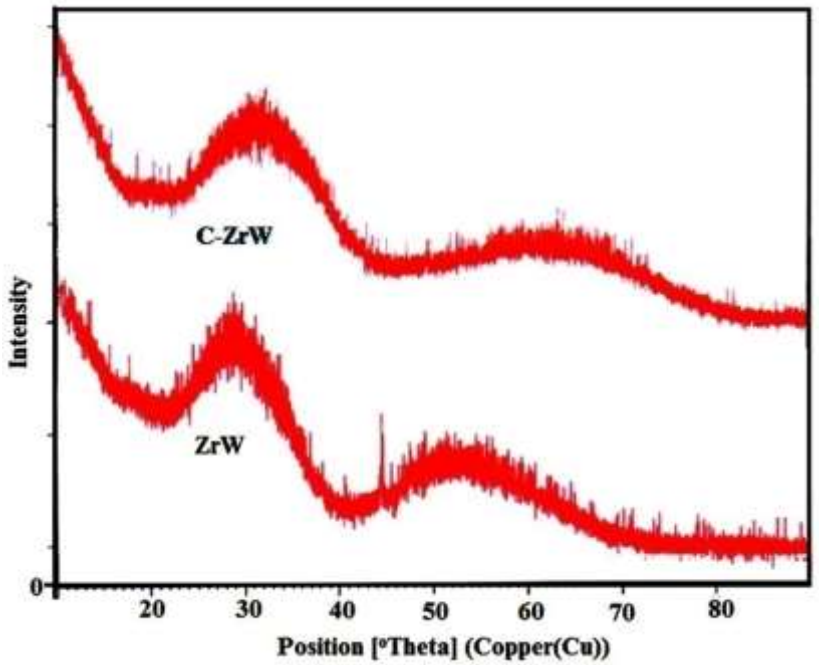

Figure 6.5 X-ray diffraction pattern of ZrW and CZrW

Figure6.5 shows the X-ray diffraction pattern of both ZrW and CZrW indicating their amorphous nature. This is in contrast to the nanoparticles prepared by P. Badrinarayanan et al. by sol gel as well as hydrothermal routes wherein they had obtained crystalline phases [47]. The diffraction pattern of ZrW is similar to amorphous zirconium tungstate reported by C.A. Perottoni et al. [48]. All the peaks (25^o, 58^o) can be assigned to amorphous ZrW_2O_8. The peaks have been broadened in the case of CZrW which shows the interaction between ZrW and Chitosan to form composite. Analysis of the Bragg's peaks was undertaken to calculate the crystallite size using the Scherrer formula (Chapter 2 section 2.2.5). The averageparticle size obtained from XRD data for ZrW and CZrW is found to be about 44.07 nm and 27.54 nm.

6.3.5 Thermogravimetric analysis

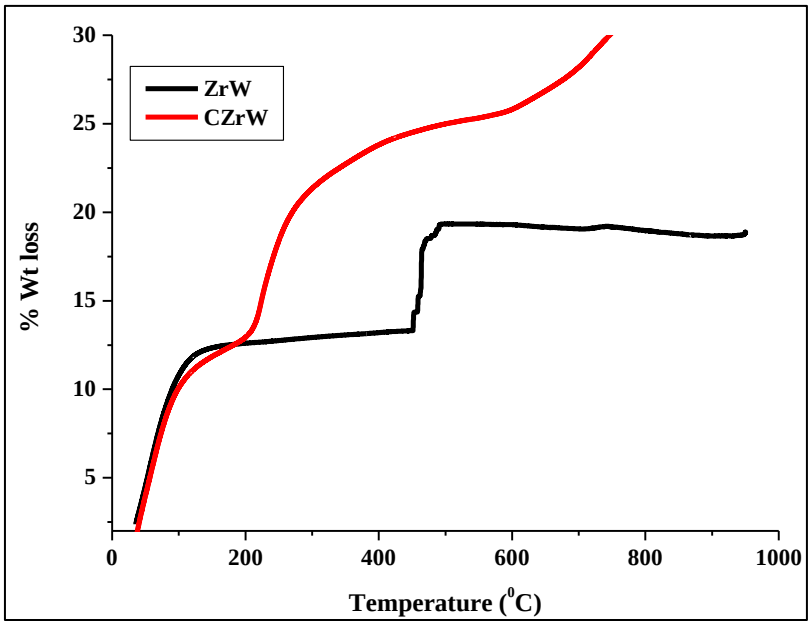

Figure 6.6 Thermogravimetriccurves of ZrW and CZrW

Figure 6.6 shows the thermal stability and degradation behaviour of ZrW and C-ZrW evaluated by TGA under nitrogen atmosphere. The total weight loss in ZrW was seen to be approximately 18%, while a weight loss of about 32 % was observed for C- ZrW. About 11-12% loss in weight occurred in the temperature range 50-110 ^{o}C followed by a stable phase and another weight loss of 6-7% at 475-480 ^{o}C. The weight loss in the narrow temperature range is consistent with a distinct dehydration event leading to a change in crystal structure [47] The TGA of CZrW

shows mainly three stage of weight loss. The first weight loss of 10-12% at 50-130 ^{o}C could be attributed to absorbed or bound water molecules. The further weight loss of about 11-12% at 240 ^{o}C is due to unbounded chitosan may be present in the composite. Another weight loss of 8-9% was observed from 470-750 ^{o}C due to further decomposition of structure [29].

6.3.6 DSC analysis

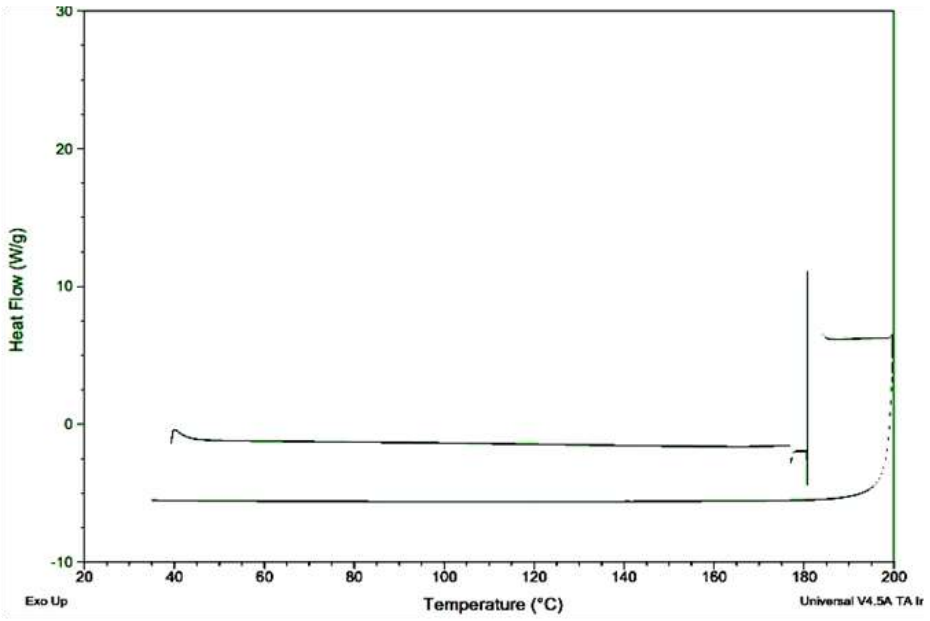

Figure 6.7 DSC thermogram of ZrW

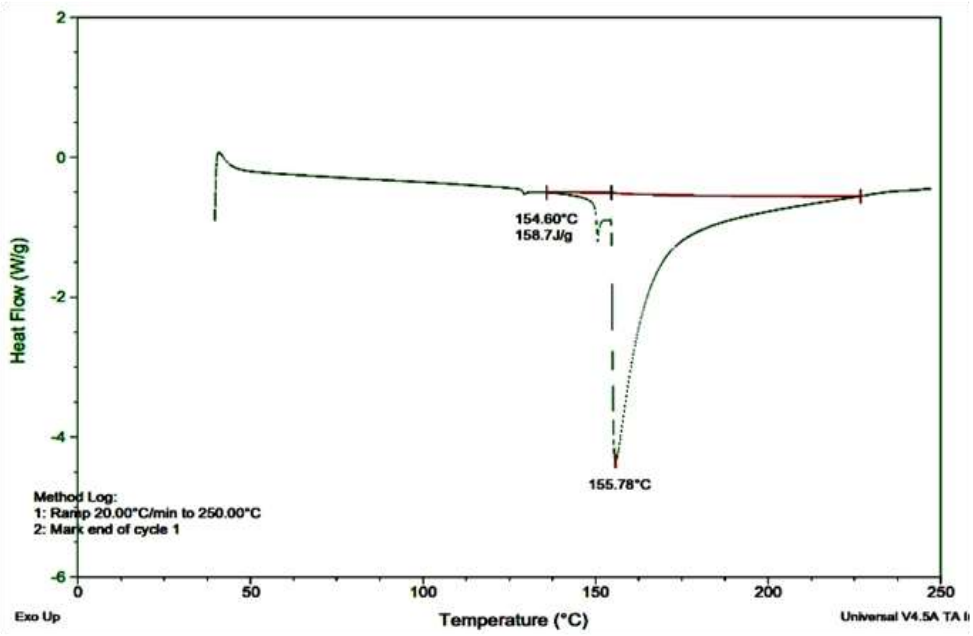

Figure 6.8 DSC thermogram of ZrW

Figure 6.7 and 6.8 show the DSC thermogram of ZrW and CZrW . The glass transition signal was observed between 175-180 ^{0}C followed by an entropy increase which can be attributed to the crystallisation of ZrW_2O_8 powders [49]. An entropy increase during the amorphous-to-crystallinetransition of zirconium tungstate was also reported by Perottoni et al [46].

However such a phenomenon was not observed when zirconium tungstate was incorporated into chitosan forming a composite. It was observed that for CZrW exhibits glass transition at 154.6^{0}C. The enthalpy associated with this transition was found to be 158.7 J/g. This was followed by an endotherm at 155.7 °C. The phase transition was no longer exothermic [50].

6.3.7 Raman spectrometric analysis

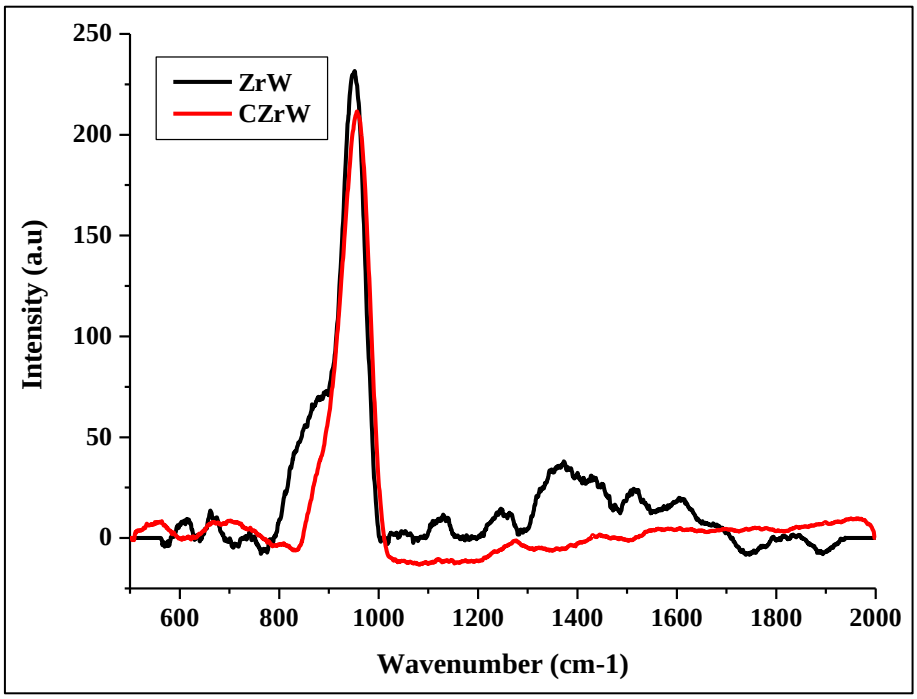

Figure 6.9 Raman spectra of ZrW and CZrW

Figure 6.9 shows the Raman spectra of ZrW and CZrW. The Raman peaks are weak due to fluorescence [51]. The Raman peaks at 1131 and 951cm^{-1} arise from symmetric stretching vibrationsof the oxygen atom around the tungsten atom in the WO_4tetrahedra, while the peaks between 951 and 740cm^{-1} can be attributed to asymmetric stretching vibrations [52, 53]. The absence of peaks at 718cm^{-1} and at ~ 805 cm^{-1} indicates the absence of tungsten oxide [45].

6.3.8 Degradation experiments

The degradation of individual (RB-21, RR-141 and Rh-6G) and mixture of dyes (RB+RR, RB+RH and RR+RH) was studied using ZrW and CZrW nanocomposites as catalysts in the presence of H_2O_2 at room temperature. Figure 6.10 and Figure6.11 shows the UV spectra for degradation of individual dyes.It was observed that 94% of RB-21, 93 % of RR-141 and 48% of Rh-6G degraded in the presence of ZrW as catalyst after keeping for a maximum time interval of 24hwhile 98 % of RB-21, 99 % RR-141 and 84% of Rh6G degraded using CZrW as catalyst. The degradation kinetics was also faster with CZrW as compared to ZrW. This could be attributed to tendency of adsorption of dyes onto chitosan matrix which could accelerate the degradation process. Figure 6.12 and Figure 6.13 show the degradation behaviour of mixture of dyes. It was observed that degradation rate and efficiency increased in binary dye mixtures RB+RH, RR+RH and RB+RR. Degradation experiments were performed in the presence of sunlight (Figure 6.14 and Figure 6.15) using ZrW and CZrW as catalysts. It was observed that complete degradation occurred for Rh-6G as well as binary mixture of dyes in a very short interval of about 5 minutes.

Blank experiments were also done to check the catalytic activity of only H_2O_2 in the absence of nanocomposite and it was observed that H_2O_2 does not play any role in the degradation of dyes. This investigation of mixture of dyes can be compared with real effluents. The catalyst was washed and dried at room temperature for further degradation experiments. The catalyst was efficient for three cycles (Figure 6.16) after which there was a slight decrease in efficiency.

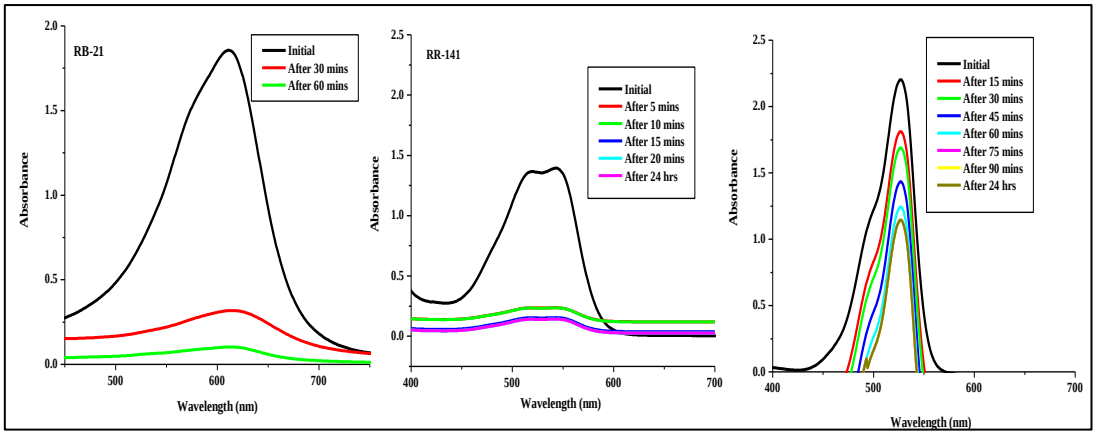

Optimum parameters - RT; Concentration 100 ppm, 3 mL; 0.5 mg catalyst; 200 µL H_2O_2

Figure 6.10 Degradation of RB-21, RR-141 and Rh-6G at room temperature in the presence of H_2O_2using ZrW as a catalyst

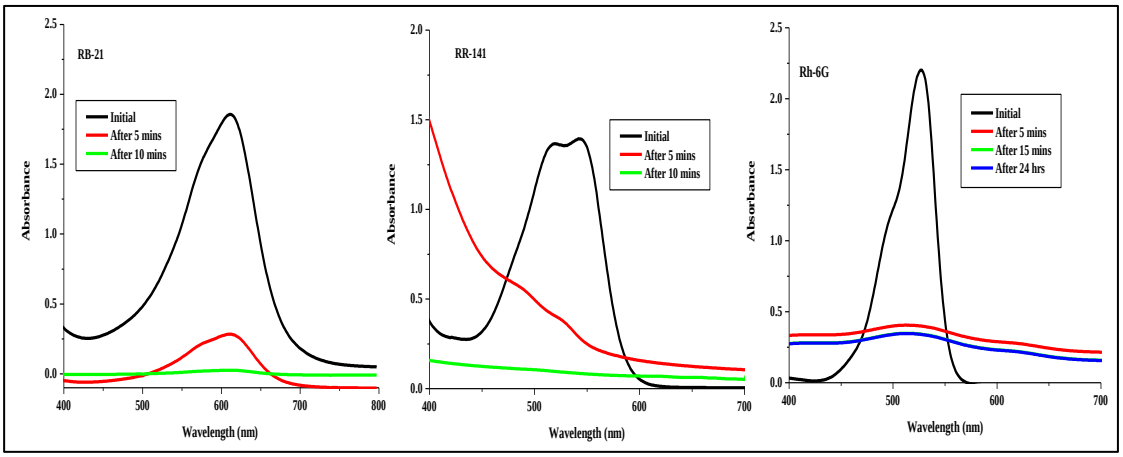

Optimum parameters - RT; Concentration 100 ppm, 3 mL; 0.5 mg catalyst; 200 µL H_2O_2

Figure 6.11 Degradation of RB-21, RR-141 and Rh-6G at room temperature in the presence of H_2O_2 using CZrW as a catalyst

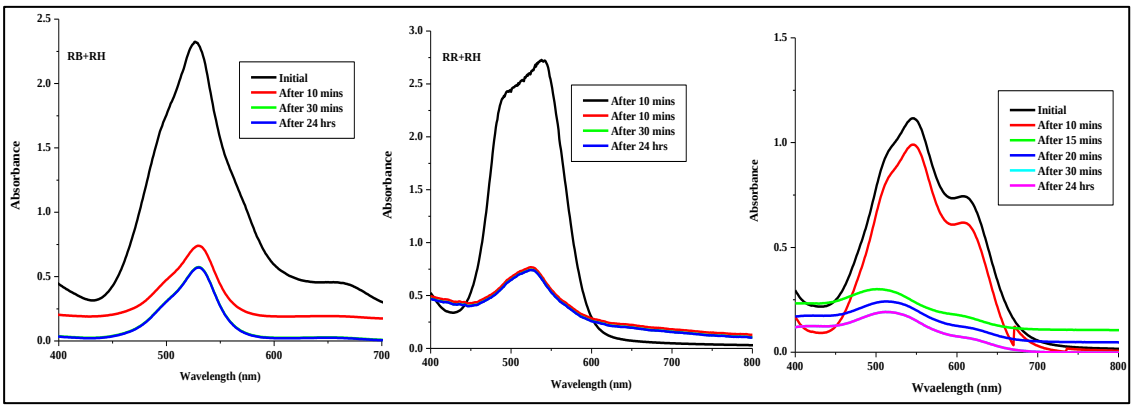

Optimum parameters - RT; Concentration 100 ppm, 3 mL; 0.5 mg catalyst; 200 µL H_2O_2

Figure 6.12 Degradation of mixture of dyes at Room temperature in the presence of H_2O_2 using ZrW as a catalyst

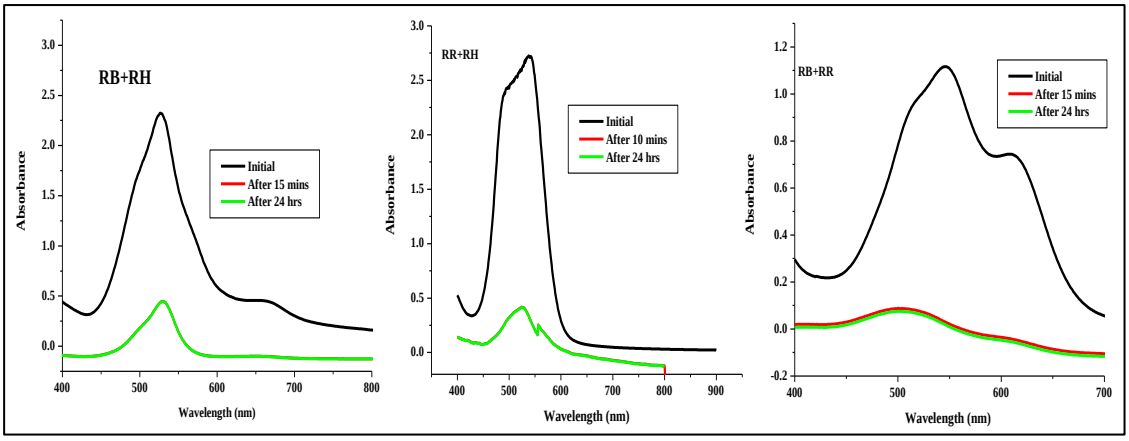

Optimum parameters - RT; Concentration 100 ppm, 3 ml; 0.5 mg catalyst; 200 µL H_2O_2

Figure 6.13 Degradation of mixture of dyes at Room temperature in the presence of H_2O_2usingCZrW as a catalyst

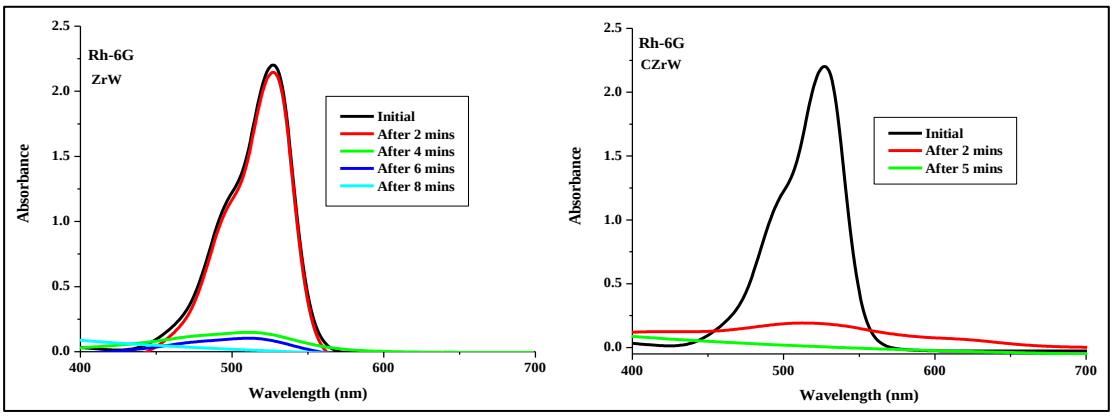

Optimum parameters - RT; Concentration 100 ppm, 3 mL; 0.5 mg catalyst; 200 µL H_2O_2

Figure 6.14 Degradation of Rhodamine 6G in the presence of sunlight and H_2O_2 using ZrW and CZrW as a catalyst

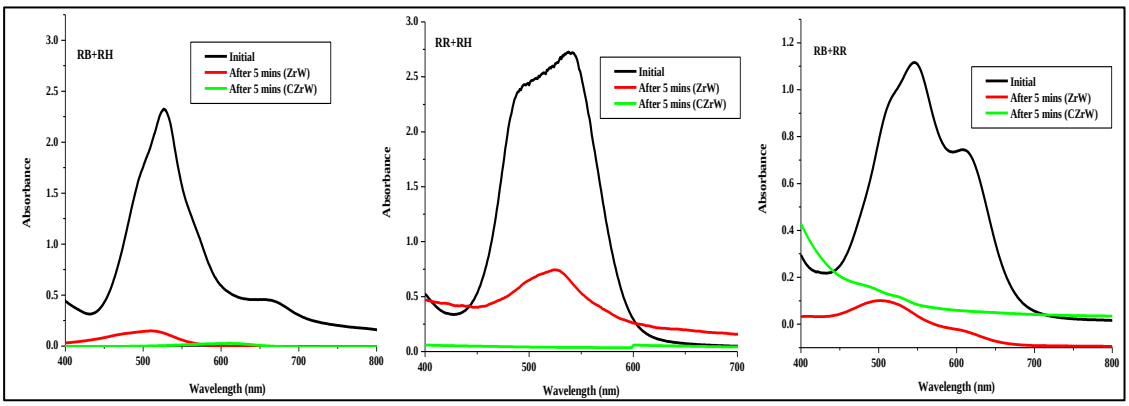

Optimum parmeters - RT; Concentration 100 ppm, 3 mL; 0.5 mg catalyst; 200 µL H_2O_2

Figure 6.15 Degradation of mixture of dyes in the presence of sunlight and H_2O_2 using ZrW and CZrW as a catalyst

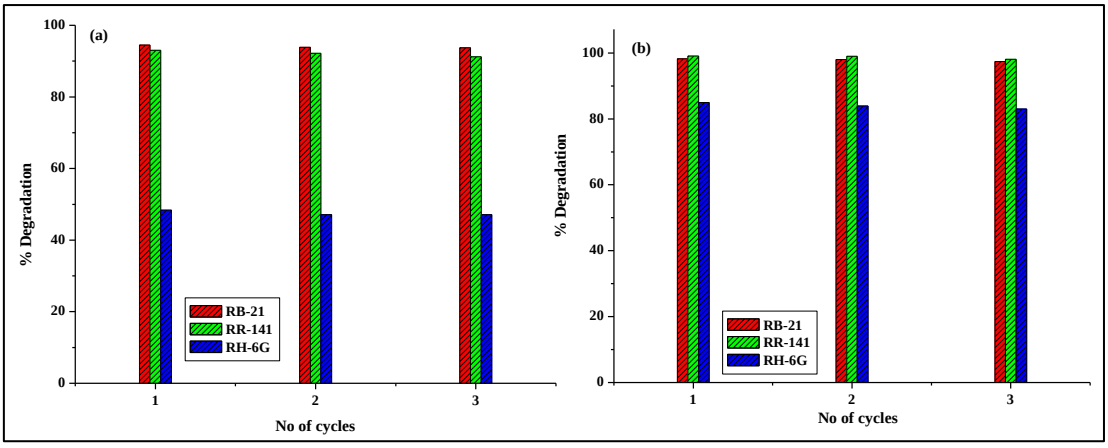

Figure 6.16 Catalyst reusability studies of a) ZrW b) CZrW

6.3.9 TOC analysis

The mineralization of organic carbon of the dyes in single component systems or in binary components (Figure 6.17) was investigated by the Total Organic Carbon (TOC) measurements.The colourless solution after degradation was analysed for TOC to see the extent of mineralisation. The TOC values show a decrease which indicates that mineralization has taken place. It was observed that mineralisation capacity was greater for ZrW as compared to CZrW. The TOC values with respect to ZrW and CZrW is 47%, 26%; 36%, 27% and 71%, 34% for RB-21, RR-141 and Rh6G respectively in single component system and. 26%, 13%; 27%, 20% and 34%, 24% for RB+RH, RR+RH and RB+RR respectively in binary systems. The TOC reduction was lesser than decolorization which may be due to the formation of smaller uncoloured products.

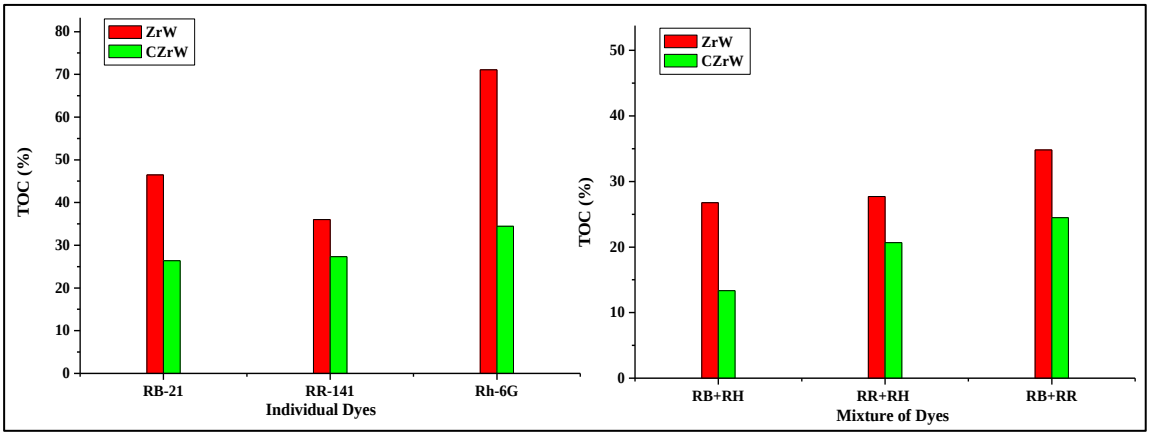

Figure 6.17 TOC analysis of after degraded dyes using ZrW and CZrW

6.3.10 Proposed Mechanism involved in the degradation process

There could be different pathways responsible for degradation and mineralisation of dyes using ZrW and CZrW.

Addition of peroxide to zirconium tungstate could result in the formation of peroxo complexes at the surface of ZrW and CZrW, which serve as visible light absorbing sensitizers and are excited by visible light. As a result, an electron is injected from the excited state of peroxide complexes to the conduction band, thereby generating $O_2^{\bullet -}$ radical possessing strong oxidation ability to initiate the degradation of dyes as discussed in chapter5. This process could explain the degradation of dyes at ambient laboratory conditions in day light (not kept in outside sunlight) though the band gap energy of ZrW and CZrW were large [54]. The semiconducting ZrW could also utilize the incident light energy to excite its electrons from valence band toconducting band; thus, leaving behind a hole. This hole may abstract an electron from hydroxyl ions togenerate hydroxyl radicals. These hydroxyl radicals will then oxidize the dye to its products. Furthermore it was observed that CZrW has more catalytic effect. This might be due to immobilization of ZrW onto the biopolymer Chitosan which improves the surface property and induces the production of hydroxyl radicals which oxidise the dye molecules for complete mineralization.

6.4 Conclusions

Quantum dot sized clusters of ZrW and CZrW were obtained by hydrothermal synthesis in an autoclave. The individual and binary mixture of dyes could be degraded using ZrW and CZrW in the presence of H_2O_2indicating their catalytic ability. It was observed that the CZrW was more effective in degradation of dyes as compared to ZrW, though ZrW was more efficient in mineralization. The absorption edge for ZrW was found to be at high energy indicating that it isa n-type semiconductor suitable for device applications which use metaloxide semiconductor such as gas sensors, UV sensors, etc.The fast and efficient photo degradation of the dyes in sunlight suggested that ZrW and CZrW could be used as efficient photocatalyst for environmental remediation.

References

[1] M.H. Habibi, N. Talebian, *Dyes Pigm.* 73**(2007)** 186.

[2] O. A. Makhotkina, S. V. Preis and E. V. Parkhomchuk, *Appl. Catal. B* 84 **(2008)**821.

[3] W. Luo, L. Zhu, N. Wang, H. Tang, M. Cao and Y. She, *Environ. Sci. Technol.* 44 **(2010)**1786.

[4] A. Rodrıguez, G. Ovejero, J. L. Sotelo, M. Mestanza and J. Garci,*Ind. Eng. Chem. Res.* 49 **(2010)**498.

[5] S. Papi, D. Vujevi, N. Koprivanac and D. Sinko, *J. Hazard.Mater.*164 **(2009)**1137.

[6] O. Gulnaz, A. Kaya, F. Matyar, B. Arikan, *J. Hazard. Mater.*108 **(2004)**183.

[7] J. Liquiang, S. Xiaojun, J. Shang, C. Weimin, X. Zili, *Sol. Energy Mater. Sol. Cells* 70 **(2003)** 133.

[8] R. Jain, S. Shirkarwar, *J. Hazard.Mater.* 152 **(2008)** 216.

[9] X. Yang, X. Cheng, H. Li, J. Xu, X. Sun,*J. Ceram. Soc. Jpn.* 116 **(2008)**471.

[10] L. Sun, A. Sneller, P. Kwon, *Compos. Sci. Technol.* 68 **(2008)** 3425.

[11] L.L.Y. Chang, M.G. Scroger, B. Phillips, *J. Am. Ceram. Soc.* 50**(1967)**211.

[12] K. de Buysser, P. Lommens, C. de Meyer, E. Bruneel, S. Hoste,I.VanDriessche, *Ceram. Silik*. 48 **(2004)** 139.

[13] T.A. Mary, J.S.O. Evans, T. Vogt, A.W. Sleight, *Sci.* 272 **(1996)**90.

[14] W. Miller, C.W. Smith, P. Dooling, A.N. Burgess, K.E. Evans, *Phys. Status Solidi.* 245 **(2006)** 552.

[15] K. J. Haman, P. Badrinarayanan, M.R. Kessler, *ACS App. Mat. Int.* 1 **(2009)** 1190.

[16] C. Lind, M.C. Coleman, L.C. Kozy, G.R. Sharma, *Phys. Status Solidi. B* 248**(2011)** 123**.**

[17] P. Badrinarayanan, B.C. Macmurray, M.R. Kessler, *J. Mater. Res.* 24 **(2009)** 2235.

[18] X. Yang, X. Cheng, H. Li, J. Xu, X. Sun,*J. Ceram. Soc. Jpn.* 116 **(2008)**471.

[19] L. Sun, A. Sneller, P. Kwon, *Compos. Sci. Technol.* 68 **(2008)** 3425.

[20] H. Holzer, D.C. Dunand, *J. Mater. Res.* 14**(1999)** 780.

[21] M. Kofteros, S. Rodriguez, V. Tandon, L.E. Murr, *Scr. Mater.* 45 **(2001)** 369.

[22] Li Jiang, Qizhao Wang, Caolong Li, Jian Yuan, W. Shangguan, *Int. J. Hydrogen Energy*35 **(2010)** 7043.

[23] L.M. Sullivan, C.M. Lukehart, *Mater.* 17 **(2005)** 2136.

[24] L. Zhang, J.Y. Howe, Y. Zheng, H. Fong, *Cryst. Growth Des.* 9 **(2009)**667.

[25] X. Xing, Q. Xing, R. Yu, J. Meng, J. Chen, G. Liu, *Physica B* 371 **(2006)** 81.

[26] L.C. Kozy, M.N. Tahir, C. Lind, W. Tremel, *J. Mater. Chem.* 19 **(2009)**2760.

[27] O. Gulnaz, A. Kaya, F. Matyar, B. Arikan, *J. Hazard. Mater.*108 **(2004)**183.

[28] C.A. Perottoni, J.A.H. da Jornada, *Science.* 280 **(1998)** 886.

[29] A.S. Pereira, C.A. Perottoni, J.A.H. da Jornada, *J. Raman Spectrosc*. 34 **(2003)** 578.

[30] C. Closmann, A.W. Sleight, J.C. Haygarth, *J. Solid State Chem.* 139 **(1998)**424.

[31] U. Kameswari, A.W. Sleight, J.S.O. Evans, *Int. J. Inorg. Mater.* 2 **(2000)** 333.

[32] C. Lind, A.P. Wilkinson, *J. Sol–Gel Sci. Technol*. 25 **(2002)** 51.

[33] A.A. Khan, M.M Alam, *Anal. Chim. Acta*. 504 **(2004)** 253.

[34] P. Lommens, C. De Meyer, E. Bruneel, K. De Buysser, I. VanDriessche, S. Hoste, *J. Eur. Ceram. Soc.* 25 **(2005)** 3605.

[35] H. Holzer, D.C. Dunand, *J. Mater. Res.* 14 **(1999)** 780.

[36] D.K. Balch, D.C. Dunand, *Metall. Mater. Trans. A*35A **(2004)**1159.

[37] C. Verdon, D.C. Dunand, *Scr. Mater.* 36 **(1997)** 1075.

[38] L.L.Y. Chang, M.G. Scroger, B. Phillips,*J. Am. Ceram. Soc.* 50**(1967)**211.

[39] W. Hongchao, R. Mark ,and K. Michael,*ACS Appl. Mater. Interfaces* 5 **(2013)** 9478.

[40] R. Niwas, U. Gupta, A.A. Khan, K.G. Varshney, *Colloids Surf. A* 164 **(2000)** 115.

[41] V. Natrayasamy, S. Meenakshi, *J. Hazardous Mate.* 176 **(2010)** 459.

[42] M. Davis, Infrared Spectroscopy and Molecular Structure,Elsevier, **(1963)**, 318, Amsterdam.

[43] F.A. Miller, C.H. Wilkins, *Anal. Chem*.24 **(1952)** 1253.

[44] A. Sharma and A. Mishra, *Adv. Mat. Lett.* 1 **(2010)**, 59.

[45] J.S.O. Evans, T.A. Mary and T. Voget, *Chem. Mater.* 8, **(1996)**, 2809

[46] S. Manoj, B. Beena, *J. Nano- Electron. Phys*, 3 **(2011)**179

[47] P. Badrinarayanan et al. *Materials Chemistry and Physics* 131 **(2011)** 12–17.

[48] C.A. Perottoni et al. / Solid State Communications 134 **(2005)** 319–322

[49] N.E. Cusack, The Physics of Structurally Disordered Matter, IOP Publishing, Bristol, **(1987)** (p. 13)

[50] G.P. Johari, *J. Phys. Chem.* B 107 **(2003)** 9063

[51] Sun et al,*Ceramics International* 39 **(2013)** 165–170

[52] K. Haman, P. Badrinarayanan, and M. R. Kessler, *ACS Applied Materials & Interfaces,*1(2009) 1190

[53] Y.Y.Huang et.al, *Applied CatalysisA: General* 172 **(1998)** 327

[54] Yan Wang, XiangjiangMeng, Xinluan Yu, Min Zhang, Jianjun Yang, Applied Catalysis B: Environmental Volumes 138–139, 326